## EDGE ARTICLE

CrossMark
click for updates

# Galvanic replacement synthesis of Ag$_x$Au$_{1-x}$@CeO$_2$ (0 ≤ x ≤ 1) core@shell nanospheres with greatly enhanced catalytic performance†

Dapeng Liu,[a] Wang Li,[a] Xilan Feng[a] and Yu Zhang*[ab]

A galvanic replacement strategy has been successfully adopted to design Ag$_x$Au$_{1-x}$@CeO$_2$ core@shell nanospheres derived from Ag@CeO$_2$ ones. After etching using HAuCl$_4$, the Ag core was *in situ* replaced with Ag$_x$Au$_{1-x}$ alloy nanoframes, and void spaces were left under the CeO$_2$ shell. Among the as-prepared Ag$_x$Au$_{1-x}$@CeO$_2$ catalysts, Ag$_{0.64}$Au$_{0.36}$@CeO$_2$ shows the optimal catalytic performance, whose catalytic efficiency reaches even 2.5 times higher than our previously reported Pt@CeO$_2$ nanospheres in the catalytic reduction of 4-nitrophenol (4-NP) by ammonia borane (AB). Besides, Ag$_{0.64}$Au$_{0.36}$@CeO$_2$ also exhibits a much lower 100% conversion temperature of 120 °C for catalytic CO oxidation compared with the other samples.

## 1. Introduction

For heterogeneous catalysis, reactions often take place at the surface of catalysts or at the interface of hybrid catalysts, so highly active surface/interface sites will greatly favor enhancing their catalytic activities. However under harsh working conditions these nanocatalysts are apt to lose their activities gradually during cycling caused by serious surface contamination or aggregation and hence a declined adsorption–desorption capability of the substrate molecules. In most cases the noble metal catalysts could show better catalytic stability if these active components were encapsulated by inert shells to form core@shell nanostructures. To date, a series of noble metal@oxide core@shell nanostructures, including Au@TiO$_2$,[1] Au@SiO$_2$,[2] Au@ZnO,[3,4] Au@Cu$_2$O,[5,6] Pt@CeO$_2$,[7] Au@CeO$_2$ (ref. 8), *etc.*, have been successfully fabricated *via* direct coating processes or templating strategies. However, the improvement of the catalytic stability is more or less based on sacrificing the catalytic activity of catalysts due to decreased active sites. It is hard to consider the catalytic activity and stability of one catalyst at the same time, so a feasible and effective way has been developed by loading active centers on supports with more open structures such as metal organic frameworks[9–13] and porous oxides.[14] In consideration of these, they all point to an ideal core@shell nanostructure that contains an active noble metal core with a hollow structure to provide enough void spaces for reactions, has an inert shell with a suitable thickness to prevent mass transfer, and rich porosity to allow the substrate molecules passing through to easily be in contact with the active core sites. More importantly, the good synergistic effects between the core and shell components might further help improve their catalytic performance.

The green synthesis of noble metal@CeO$_2$ core@shell hybrid nanocatalysts has been a research highlight in recent years, which brings at least two remarkable advantages: (1) the facile and fast mass production to gram scale in aqueous solution without the addition of any organics; (2) a naked surface/interface as well as strong synergistic effects between the noble metal and CeO$_2$. The key principle during the synthesis should be the auto-redox reaction by activating Ce$^{3+}$ ions to reduce the high-valence-state noble metal ions, spontaneously forming the final noble metal@CeO$_2$ core@shell hybrid nanostructures.[7,15–17] For example, Kayama and coworkers reported good work on Ag@CeO$_2$ nanospheres for a catalytic CO oxidation reaction.[16,17] Before long, our group also succeeded in modulating the size of Pt@CeO$_2$ (ref. 7) and Pd@CeO$_2$ (ref. 15) nanospheres and optimizing their size-dependent catalytic properties in catalytic CO oxidation.

Besides the synthesis, creating void spaces *in situ* in the core@shell nanostructure becomes another challenge to the above-mentioned ideal structure until the development of a hard-templating strategy in combination with selective etching processes, like coordination etching[18,19] and galvanic replacement.[20–23] For the former, the etching is triggered by some kind of special intermolecular coordination interactions. Meanwhile the entropy-driven process determines the formation of the final products. Typically, the precipitate with a higher $K_{sp}$ is easy

[a] *Key Laboratory of Bio-Inspired Smart Interfacial Science and Technology of Ministry of Education, School of Chemistry and Environment, Beihang University, Beijing 100191, China. E-mail: jade@buaa.edu.cn*

[b] *International Research Institute for Multidisciplinary Science, Beihang University, Beijing 100191, P. R. China*

† Electronic supplementary information (ESI) available: Detailed synthesis, XRD patterns, EDX and XPS spectra of Ag$_x$Au$_{1-x}$@CeO$_2$ core@shell nanospheres. TEM images of Ag@CeO$_2$, and Ag$_x$Au$_{1-x}$@CeO$_2$ prepared with addition of NaCl. See DOI: 10.1039/c5sc02774h

to be converted to another one with a lower $K_{sp}$ value. Guo's group adopted this similar principle to create a series of transition meal oxide nanocages using $Cu_2O$ as the template.[18] For the latter, the redox relationship among the different kinds of substrates has also been employed, which is called a galvanic replacement reaction that happens between the oxidative metal ions and the reductive substrate. Xia *et al.* showed us excellent work on the synthesis of AgAu alloy nanoboxes, nanorattles and multi-walled nanoshells/nanotubes *via* the galvanic replacement.[20,21] Besides noble metals, such a replacement reaction has also been successfully extended to the metal oxide systems. The current representative result confirms that the replacement reaction can be triggered between $Mn_3O_4$ and $Co^{2+}$, resulting in hollow $Co_3O_4$ nanocages.[22]

After careful consideration, the galvanic replacement reaction was thought to be suitable for designing the above-mentioned ideal core@shell structures. It is noticed that the reduction potentials of $Ag^+/Ag$ and $AuCl_4^-/Au$ pairs are 0.80 V and 0.99 V *vs.* SHE, respectively. Such a potential difference makes it feasible to replace Ag components by Au through the galvanic replacement reaction between $AuCl_4^-$ and $Ag^0$. Additionally, one $Au^{III}$ ion could oxidize three $Ag^0$ atoms, resulting in $Ag_xAu_{1-x}$ alloy nanoframes if the Ag core was etched partially. So the issues are now focused on how to prepare the $Ag@CeO_2$ nanospheres and how to control the replacement reaction to obtain the desired $Ag_xAu_{1-x}@CeO_2$ nanospheres from the viewpoint of material design.

In this paper, we demonstrate a green auto-redox reaction between $AgNO_3$ and $Ce(OH)_3$ for the synthesis of $Ag@CeO_2$ nanospheres as templates, and then adopt the galvanic replacement strategy to oxidize the Ag core in order to prepare the final $Ag_xAu_{1-x}@CeO_2$ nanospheres. No organics were introduced into this reaction system during the whole synthetic process as shown in Scheme 1. After systematic structure characterization, the catalytic performance of the $Ag_xAu_{1-x}@$-$CeO_2$ samples was also evaluated using the two typical model reactions of catalytic reduction of 4-NP by AB and catalytic CO oxidation.

## 2. Results and discussion

### 2.1 Structure characterization

$Ag@CeO_2$ core@shell nanospheres were prepared according to a previous report except for some modification.[16,17] Here, we increase the molar ratio of Ce/Ag from 2/3 to 1/1 so as to realize a more compact encapsulation of $CeO_2$ on Ag cores. The
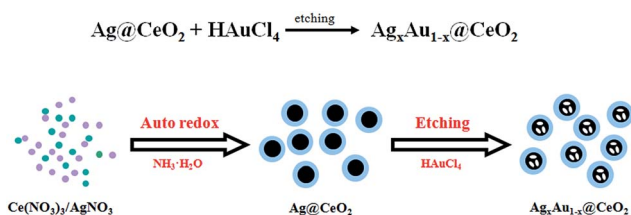
transmission electron microscopy (TEM) images in Fig. S1† show that every $Ag@CeO_2$ core@shell nanosphere is composed of an Ag core with an average size of 45 nm and a close-packed shell of 5 nm-sized $CeO_2$ nanoparticles.

After introducing $HAuCl_4$ into the solution, the galvanic replacement reaction was triggered. As shown in the TEM image (Fig. 1A), the final products well maintained the original monodispersed sphere-like morphology. However, the enlarged TEM image (Fig. 1B) clearly shows that the initial Ag cores began to become void, indicating the successful etching process. EDX analysis (Fig. S2†) provides the affirmative proof of the presence of an Au signal beside the original ones of Ag and Ce elements. The molar ratio of Ag/Au determined using ICP is 0.64/0.36, so we abbreviate this Ag rich product as $Ag_{0.64}Au_{0.36}@CeO_2$. If the feeding amount of $HAuCl_4$ was further increased, the Au-rich products should be produced. As expected, when the amount of $HAuCl_4$ was increased from 0.3 to 0.6 mL, the initial solid Ag cores were etched more deeply, which left obvious voids without breaking the external morphology of these nanospheres and changed their size as observed from the TEM images (Fig. 1C and D). After the determination using ICP, the Au-rich product was named as $Ag_{0.41}Au_{0.59}@CeO_2$ according to the Ag/Au ratio. From the powder X-ray diffraction (XRD) patterns of the $Ag_xAu_{1-x}@CeO_2$ samples in Fig. S3,† it can be seen that the diffraction peaks at $2\theta = 28.6°, 33.1°, 47.3°$ and $56.4°$ are in good accordance with the standard diffraction peaks of the fluorite-phase $CeO_2$ crystals, while the other diffraction peaks at $2\theta = 38.2°, 44.3°, 64.5°$ and $77.6°$ could be attributed to the noble metal cores. However, owing to the structural similarity between Ag and Au, it is hard to directly distinguish the shift of $Ag_xAu_{1-x}$ alloys compared with pure Ag or Au. However, the intensity of the peak at $38.2°$ obviously increased with the larger
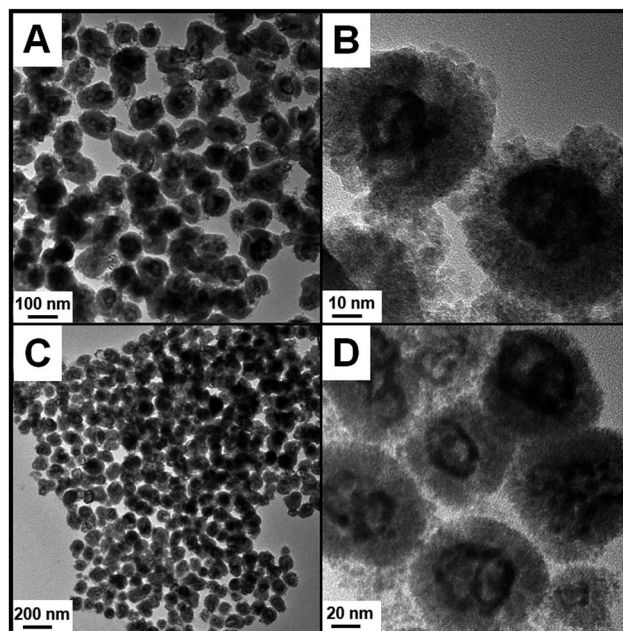


**Scheme 1** Synthetic strategy for $Ag_xAu_{1-x}@CeO_2$ core@shell nanospheres.



**Fig. 1** TEM images of $Ag_{0.64}Au_{0.36}@CeO_2$ (A and B) and $Ag_{0.41}$-$Au_{0.59}@CeO_2$ (C and D).

content of Au. In combination with the EDX spectrum (Fig. S4†), the X-ray photoelectron spectroscopy (XPS) (Fig. S5 and S6†) and ICP analyses can confirm the successful formation of the AgAu alloys instead of the pure Ag cores.

If excess $HAuCl_4$ was added in the reaction solution, the thoroughly replaced product of $Au@CeO_2$ core@shell nanospheres could be obtained. TEM images in Fig. 2A and B show that for each nanosphere the shell part is still built up of sub-5 nm $CeO_2$ nanoparticles. The Au core beneath the shell can be distinguished by their deeper contrast from $CeO_2$. However, a sub-30 nm Au particle as a single core, rather than the initial 45 nm sized Ag, is located in the center of the $CeO_2$ aggregates. The high-angle annular dark-field scanning transmission electron microscopy (HAADF-STEM) images (Fig. 2C–E) effectively show the distribution of the Au and Ce components in the nanospheres and that the Ce element spreads everywhere and Au only exists in the center of the nanosphere. No Ag signal can be detected, indicating that the replacement reaction is quite complete. The XRD pattern of the as-obtained sample (Fig. S3†) matches well with those of $Ag@CeO_2$, $Ag_{0.64}Au_{0.36}@CeO_2$, and $Ag_{0.41}Au_{0.59}@CeO_2$. The XPS spectra (Fig. S7†) identify that the two peaks at 349.9 eV and 340.4 eV correspond well to the Au $3d_{5/2}$ and $3d_{3/2}$ spin orbit peaks of Au, respectively, while the peaks at 881.9 eV and 900.2 eV can be assigned to Ce $3d_{5/2}$ and $3d_{3/2}$ spin orbit peaks, respectively.

## 2.2 Influence on the structure evolution

According to the references, the galvanic replacement of Ag by $HAuCl_4$ proceeds as follows:

$$Ag + HAuCl_4 \rightarrow Au\downarrow + AgCl\downarrow$$
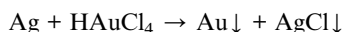
Two scenarios often appeared during the similar fabrication of $Ag_xAu_{1-x}$ alloy nanoframes, that is, (1) Au nucleates independently in the solution rather than on the initial Ag nanostructures; (2) Au crystallizes on the exposed Ag faces or on the



**Fig. 2** TEM (A and B), and HAADF–STEM images (C to E) of $Au@CeO_2$.

edge of the Ag nanostructures. We notice that in our case the $Ag@CeO_2$ template is in a core@shell structure which should not be good for effectively removing the byproduct of AgCl precipitation from the core position during the reaction, so a large excess of NaCl was introduced to dissolve the produced AgCl.[24] However, it is unexpected that the original Ag cores disappeared as well and left hollow $CeO_2$ nanospheres. Meanwhile, most of the Au nanoparticles actually nucleated on the outer face of the $CeO_2$ shell as shown in Fig. S8.† Moreover, such a self-nucleation tendency became stronger when further increasing the feeding amount of $HAuCl_4$. The galvanic replacement reaction was obviously out of control. The following reasons are supposed to account for the undesired result. Firstly, the $CeO_2$ shell, as a hard template, limited the core space that couldn't provide enough room to stand the volume expansion during the galvanic replacement reaction. Since the constantly produced AgCl would occupy the core before dissolving, Au had to nucleate on the outer surface of the $CeO_2$ shell. Secondly, referenced to a previous report,[16] it is found that the aggregated $CeO_2$ shell of $Ag@CeO_2$ might be not enclosed enough, leaving a possible route for the overflow of Au. So two improvements to the synthesis were developed to optimize the galvanic replacement reaction: (1) increasing the feeding molar ratio of Ce/Ag from 2/3 to 1/1 to make the $CeO_2$ shell packed more compactly so as to prevent Au from overflowing; (2) introducing excess $NH_4Ac$ along with NaCl. The co-presence of $NH_4Ac$ and NaCl was identified as more effective for the dissolution of the AgCl precipitate to provide enough core space for the growth of Au, though under the more compact $CeO_2$ shell.

## 2.3 Catalytic test

**2.3.1 Catalytic reduction of 4-NP by AB.** To evaluate the catalytic performance of the four samples of $Ag@CeO_2$, $Ag_{0.64}Au_{0.36}@CeO_2$, $Ag_{0.41}Au_{0.59}@CeO_2$ and $Au@CeO_2$, a safer hydrogenation reaction was chosen here using AB instead of the dangerous $NaBH_4$ or $H_2$ as the reductant in the catalytic liquid-phase reduction of 4-NP. The reaction was conducted with the molar ratio of 4-NP/AB/catalyst as 1/100/0.2. AB was used in a large excess here compared to 4-NP. Given the constant concentration of AB during the reaction, the reduction rate can be thus evaluated using pseudo-first-order kinetics with respect to 4-NP. The whole catalytic process was monitored using UV-vis spectroscopy. Before detection, 4-NP was first treated with NaOH (4-NP/NaOH = 1/1 in molar ratio) to complete its protonation process. Accordingly, the original faint yellow solution became deep yellow (its characteristic absorption peak is at 400 nm). The following introduction of AB caused almost no change to be observed from the corresponding UV-vis spectra, indicating that 4-NP did not react with AB in the absence of the catalysts at ambient conditions. However, a large number of bubbles suddenly appeared around the catalysts if added, and the deep yellow solution faded in minutes. As shown in Fig. 3 for $Ag@CeO_2$, the intensity of the absorption peak at 400 nm decreased very slowly so that after 10 min only about 95% 4-NP were converted to 4-aminophenol (4-AP). However,

$Ag_{0.64}Au_{0.36}@CeO_2$ and $Ag_{0.41}Au_{0.59}@CeO_2$ exhibited much higher activities, which could catalyze the 100% conversion of 4-NP into 4-AP in 4 min and 6 min, respectively. The activities of the four samples follow the sequence $Ag_{0.64}Au_{0.36}@CeO_2 >$ $Ag_{0.41}Au_{0.59}@CeO_2 \gg Au@CeO_2 > Ag@CeO_2$. The approximate TOF, which is defined as the number of moles of reduced 4-NP per mole of noble metal atoms per minute when the conversion reached 90%, has been used to compare the catalytic activities of the four samples. As shown in Fig. 3B, the TOF value of $Ag_{0.64}Au_{0.36}@CeO_2$ is 3.5 $min^{-1}$, which is about 2.5 times higher than our previously reported $Pt@CeO_2$ catalyst.[7] The detailed data are shown in Table S1.†

**2.3.2 Catalytic CO oxidation.** Furthermore, the catalytic performance of the as-obtained $Ag_xAu_{1-x}@CeO_2$ nanospheres has also been evaluated in another model reaction of CO oxidation. All of the four samples were dried into powders before use without a further optimizing treatment. Fig. 4A shows the typical conversion ratio of CO as a function of the reaction temperature under the conditions that the feed gas containing 1 vol% CO and 99 vol% air is allowed to pass through the reactor at a total flow rate of 30 mL $min^{-1}$. As seen, $Au@CeO_2$ exhibits the worst catalytic performance and even when the reaction temperature was increased to 300 °C, only about 90% of CO was oxidized to $CO_2$. Meanwhile, $Ag@CeO_2$ showed a higher catalytic activity and its $T_{100}$ (100% conversion temperature) is 200 °C. However, the $T_{100}$ values of $Ag_{0.64}Au_{0.36}@CeO_2$ and $Ag_{0.41}Au_{0.59}@CeO_2$ markedly decrease to about 120 °C and 150 °C, respectively. The aging test (Fig. 4B) shows that $Ag_{0.64}Au_{0.36}@CeO_2$ deteriorates only a little in CO conversion even after continuously working for five hours, indicating its good catalytic stability.

**2.3.3 Discussion of the catalytic performance.** The as-obtained $Ag_xAu_{1-x}@CeO_2$ nanospheres have been evaluated using the two model reactions of the catalytic reduction of 4-NP by AB and catalytic CO oxidation. Obviously $Ag_xAu_{1-x}$ alloy nanoframes performed better than either pure Ag or Au. The different catalytic performances of these samples might be
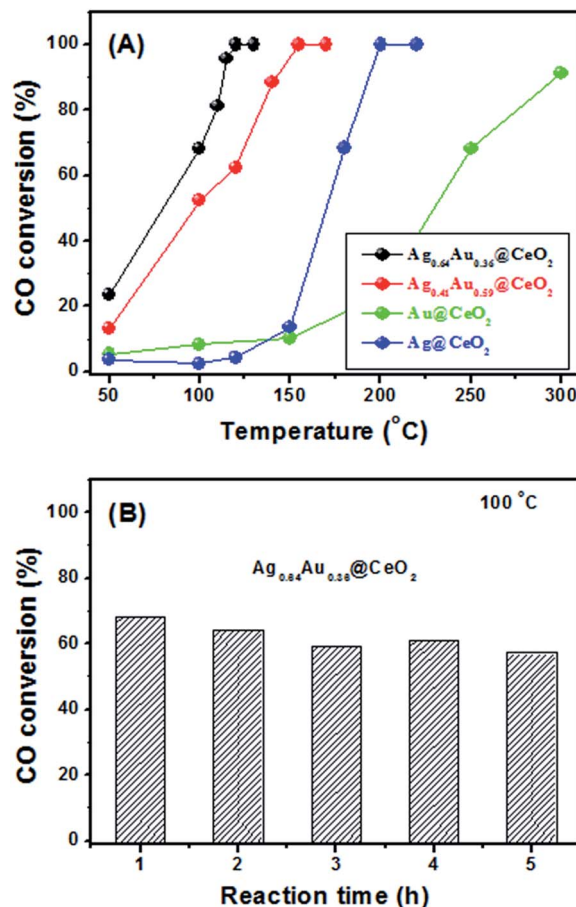


Fig. 4  (A) CO conversion curves of $Ag@CeO_2$, $Ag_{0.64}Au_{0.36}@CeO_2$, $Ag_{0.41}Au_{0.59}@CeO_2$ and $Au@CeO_2$; (B) cycling test of $Ag_{0.64}Au_{0.36}@-CeO_2$ at 100 °C for 5 h.

composition and structure dependent. As reported, the compositions of noble metals can strongly affect their catalytic performance. For instance, it has been identified that AuPd,[25] AgPd,[26] RhPt,[27] PdPt,[28,29] etc. alloy nanostructures often exhibit enhanced catalytic activity compared to their individual components due to synergistic effects and the rich diversity of the compositions. There are several merits of these alloy nanostructures prepared via galvanic replacement, which make them promising for catalytic applications: (1) the presence of inner surfaces and porous walls endow them with much larger reactive surface areas than the solid ones; (2) the alloyed structure endows them with good flexibility and stability. (3) The large surface favors the efficient electrical connections in the redox system. (4) The facilely tuned compositions allow for optimizing the catalytic performance for given reactions.[30–32]

In this work, the Ag rich sample of $Ag_{0.64}Au_{0.36}@CeO_2$ shows the optimal catalytic property compared with others. This result firmly proves that composition is a main factor for the catalytic performance. Besides, the hollow core@shell nanostructures of $Ag_{0.64}Au_{0.36}@CeO_2$ and $Ag_{0.41}Au_{0.59}@CeO_2$ are believed to be another key factor to influence their activities, because enough voids would facilitate the contact of 4-NP and AB on the surface of the $Ag_xAu_{1-x}$ alloy nanoframes more easily, favoring the fast
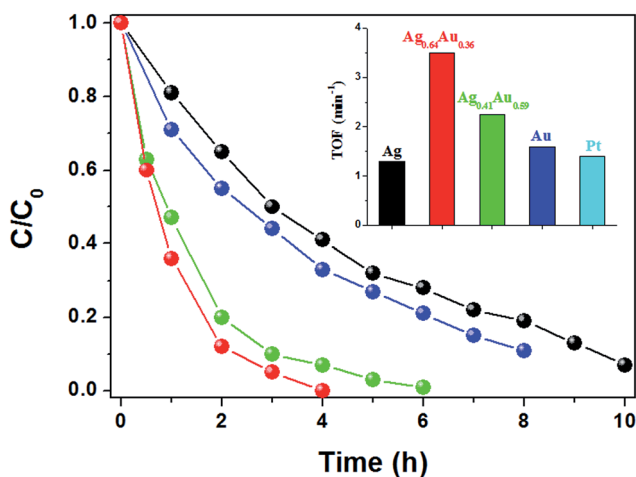


Fig. 3  Catalytic reduction of 4-NP by $Ag@CeO_2$ (black), $Ag_{0.64}-Au_{0.36}@CeO_2$ (red), $Ag_{0.41}Au_{0.59}@CeO_2$ (green) and $Au@CeO_2$ (blue). Inset: calculated TOF compared with $Pt@CeO_2$.[7]

diffusion of the reactants and the final products through the $CeO_2$ shell as described by Tang et al.[33]

## 3. Conclusions

Overall, we have successfully prepared uniform $Ag@CeO_2$ core@shell nanospheres via the auto-redox reaction that was triggered between $Ce(OH)_3$ and $AgNO_3$ in aqueous solution. The whole synthesis process is totally clean without using any organic solvent, redox reagent and surfactant. As a template, the as-prepared $Ag@CeO_2$ core@shell nanospheres can be facilely etched by $HAuCl_4$ to form the $Ag_xAu_{1-x}$ alloy nanoframes with hollow voids in the initial Ag core position via the in situ galvanic replacement strategy. The detailed catalytic tests show that the catalytic performance of the as-prepared $Ag_xAu_{1-x}@CeO_2$ catalysts is strongly related to their composition and structure. Among these catalysts, the Ag rich sample of $Ag_{0.64}Au_{0.36}@CeO_2$ exhibits the best catalytic activity, whose catalytic efficiency reaches even 2.5 times higher than our previously reported $Pt@CeO_2$ nanospheres in the catalytic reduction of 4-NP by AB. Moreover, $Ag_{0.64}Au_{0.36}@CeO_2$ exhibits a much lower 100% conversion temperature of 120 °C for catalytic CO oxidation, compared with $Ag_{0.41}Au_{0.59}@CeO_2$ (150 °C), $Ag@CeO_2$ (200 °C) and $Au@CeO_2$ (>300 °C). It is believed that such a fast, green, bottom-up synthetic strategy will be of great significance for the design and preparation of highly active and stable catalysts with complex compositions and hollow nanostructures.

## Acknowledgements

## Notes and references

1 J. Du, J. Qi, D. Wang and Z. Tang, Energy Environ. Sci., 2012, 5, 6914.
2 U. Jeong, J. Joo and Y. Kim, RSC Adv., 2015, 5, 55608.
3 H. Sun, J. He, J. Wang, S. Zhang, C. Liu, T. Sritharan, S. Mhaisalkar, M. Han, D. Wang and H. Chen, J. Am. Chem. Soc., 2013, 135, 9099.
4 Y. Xu, L. Chen, X. Wang, W. Yao and Q. Zhang, Nanoscale, 2015, 7, 10559.
5 C. Kuo, T. Hua and M. Huang, J. Am. Chem. Soc., 2009, 131, 17871.
6 L. Zhang, D. A. Blom and H. Wang, Chem. Mater., 2011, 23, 4587.
7 X. Wang, D. P. Liu, S. Y. Song and H. J. Zhang, J. Am. Chem. Soc., 2013, 135, 15864.
8 J. Qi, J. Chen, G. Li, S. Li, Y. Gao and Z. Tang, Energy Environ. Sci., 2012, 5, 8937.
9 A. Aijaz, A. Karkamkar, Y. Choi, N. Tsumori, E. Rönnebro, T. Autrey, H. Shioyama and Q. Xu, J. Am. Chem. Soc., 2012, 134, 13926.
10 H. Jiang, T. Akita, T. Ishida, M. Haruta and Q. Xu, J. Am. Chem. Soc., 2011, 133, 1304.
11 X. Gu, Z. Lu, H. Jiang, T. Akita and Q. Xu, J. Am. Chem. Soc., 2011, 133, 11822.
12 Q. Zhu, J. Li and Q. Xu, J. Am. Chem. Soc., 2013, 135, 10210.
13 H. Jiang, B. Liu, T. Akita, M. Haruta, H. Sakurai and Q. Xu, J. Am. Chem. Soc., 2009, 131, 11302.
14 X. Liang, J. Xiao, B. Chen and Y. Li, Inorg. Chem., 2010, 49, 8188.
15 X. Wang, D. P. Liu, J. Li, J. Zhen, F. Wang and H. J. Zhang, Chem. Sci., 2015, 6, 2887.
16 T. Kayama, K. Yamazaki and H. Shinjoh, J. Am. Chem. Soc., 2010, 132, 13154.
17 T. Mitsudome, Y. Mikami, M. Matoba, T. Mizugaki, K. Jitsukawa and K. Kaneda, Angew. Chem., Int. Ed., 2012, 51, 278.
18 J. Nai, Y. Tian, X. Guan and L. Guo, J. Am. Chem. Soc., 2013, 135, 16082.
19 Z. Wang, D. Luan, F. Boey and X. W. Lou, J. Am. Chem. Soc., 2011, 133, 4738.
20 Y. Sun and Y. Xia, J. Am. Chem. Soc., 2004, 126, 3892.
21 Y. Sun, B. Wiley, Z. Li and Y. Xia, J. Am. Chem. Soc., 2004, 126, 9399.
22 M. Oh, T. Yu, S. Yu, B. Lim, K. Ko, M. Willinger, D. Seo, B. Kim, M. Cho and J. Park, Science, 2013, 340, 694.
23 G. Gao, L. Yu, H. Wu and X. W. Lou, Small, 2014, 10, 1741.
24 J. M. Yan, Z. L. Wang, L. Gu, S. J. Li, H. L. Wang, W. T. Zheng and Q. Jiang, Adv. Energy Mater., 2015, 5, 1500107.
25 Y. Ping, J. M. Yan, Z. L. Wang, H. L. Wang and Q. Jiang, J. Mater. Chem. A, 2013, 1, 12188.
26 S. Alayoglu and B. Eichhorn, J. Am. Chem. Soc., 2008, 130, 17479.
27 L. Zhang, L. T. Roling, X. Wang, M. Vara, M. Chi, J. Liu, S. I. Choi, J. Park, J. A. Herron, Z. Xie, M. Mavrikakis and Y. Xia, Science, 2015, 349, 412.
28 J. Yang, D. Shen, L. Zhou, W. Li, X. Li, C. Yao, R. Wang, A. M. El-Toni, F. Zhang and D. Zhao, Chem. Mater., 2013, 25, 3030.
29 J. Zhen, D. Liu, X. Wang, J. Li, F. Wang, Y. Wang and H. Zhang, Dalton Trans., 2015, 44, 2425.
30 X. Xia, Y. Wang, A. Ruditskiy and Y. Xia, Adv. Mater., 2013, 25, 6313.
31 H. L. Liu, F. Nosheen and X. Wang, Chem. Soc. Rev., 2015, 44, 3056.
32 X. Hong, D. Wang, S. Cai, H. Rong and Y. Li, J. Am. Chem. Soc., 2012, 134, 18165.
33 G. Li and Z. Tang, Nanoscale, 2014, 6, 3995.